RtEstim: Effective reproduction number estimation with trend filtering

Jiaping Liu[a,1], Zhenglun Cai[b], Paul Gustafson[a], and Daniel J. McDonald[a]

[a]Department of Statistics, The University of British Columbia
[b]Centre for Health Evaluation and Outcome Sciences, The University of British Columbia

November 13, 2023

Abstract

To reveal the transmissibility of infectious diseases, epidemiologists have meticulously devoted attention to effective reproduction numbers estimation in recent years. Plenty of refined approaches have been proposed to produce accurate estimation using the data resources limited by the challenges of surveillance data collection. Arbitrary model assumptions (that are unverifiable through data) and sophisticated frameworks (that result in computational inefficiency) are critical limitations in many existing approaches. We propose a Poisson trend filtering estimator `RtEstim` for effective reproduction numbers estimation. Our `RtEstim` estimator produces accurate estimation based on the minimum requirements on available data and model assumptions with computational efficiency, especially for large-scale data. Our `RtEstim` is found empirically robust under the violation of the distributional assumption of Poisson incidences. Implementation is accessible in our lightweight `R` package `rtestim`.

Keywords: Poisson trend filtering | accurate effective reproduction number | approximate confidence bands

[1]To whom correspondence should be addressed. E-mail: jiaping.liu@stat.ubc.ca

Contents

1 Introduction

The effective reproduction number (also called the instantaneous reproduction number) is a key quantity for understanding infectious disease dynamics including the potential size of a pandemic, the required stringency of prevention measures, and the efficacy of other controls. The effective reproduction number is defined to be the average number of secondary infections caused by a new primary infection that occurs at a specific time. Tracking the time series of this quantity is therefore useful for understanding whether or not future infections are likely to increase or decrease from the current state. Let $\mathcal{R}(t)$ denote the effective reproduction number at time t. Practically, as long as $\mathcal{R}(t) < 1$, infections will decline gradually, eventually resulting in a disease-free equilibrium, whereas when $\mathcal{R}(t) > 1$, infections will continue to increase, resulting in endemic equilibrium. While $\mathcal{R}(t)$ is fundamentally a continuous time quantity, it can be related to data only at discrete points in time $t = 1, \ldots, n$. This sequence of effective reproduction numbers over time is not observable, but nonetheless is easily interpretable and retrospectively describes the course of an epidemic. Therefore, a number of procedures exist to estimate $\mathcal{R}_t$ from different types of observed incidence data such as cases, deaths, or hospitalizations while relying on various domain-specific assumptions. Importangly, accurate estimation of effective reproduction numbers relies heavily on the quality of the available data, and, due to the limitations of data collection, such as underreporting and lack of standardization, epidemiological models, estimation methodologies rely on various assumptions to compensate. Because model assumptions may not be easily verifiable from data alone, it is also critical for any estimation procedure to be robust to model misspecification.

Many existing approaches for effective reproduction number estimation are Bayesian: they estimate the posterior distribution of $\mathcal{R}_t$ conditional on the observations. One of the first such approaches is the software `EpiEstim` (Cori et al., 2020), described by Cori et al. (2013). This method is prospective, in that it uses only information available at time t in order to estimate $\mathcal{R}_t$ for $i = 1, \ldots, t$. An advantage of `EpiEstim` is its straightforward statistical model: incidence data follows the Poisson distribution conditional on past incidence and $\mathcal{R}_t$, the conjugate prior distribution for $\mathcal{R}_t$ is Gamma with fixed hyperparameters, and the serial interval distribution is fixed and known. For this reason, `EpiEstim` requires little domain expertise for use, and it is computationally fast. Thompson et al. (2019) modified this method to distinguish imported cases from local transmission and simultaneously estimate the serial interval distribution. Nash et al. (2023) further extended `EpiEstim` by using "reconstructed" daily incidence data to handle cases when the data is not regularly spaced. Abbott et al. (2020b) proposed a Bayesian latent variable framework, `EpiNow2` (Abbott et al., 2020a), which leverages incident cases, deaths or other available streams simultaneously along with allowing

additional delay distributions (incubation period and onset to report delay) in modelling. Lison et al. (2023) proposed an extension that handles missing data by imputation followed by a truncation adjustment. Parag (2021) also proposed a Bayesian approach, `EpiFilter` based the (discretized) on Kalman Filter and Smoother. `EpiFilter` also estimates the posterior of $\mathcal{R}_t$ given a Gamma prior and Poisson distributed incident cases. Compared to `EpiEstim`, `EpiFilter` estimates $\mathcal{R}_t$ retrospectively using all available incidence data both prior and subsequent to time t, and provides robust estimation in low incidence cases. Gressani et al. (2022) proposed a Bayesian P-splines approach, `EpiLPS`, that assumes negative Binomial distributed incidences. Trevisin et al. (2023) proposed a Bayesian model based on particle filtering to estimate spatially explicit effective reproduction numbers. Bayesian approaches estimate the posterior distribution of the effective reproduction numbers, and possess the advantage that the credible intervals can be easily computed. A limitation of many Bayesian approaches is that they usually require heavy computational workload, especially when observed data sequences are long or hierarchical structures are complex. Below, we compare our method to two computationally efficient Bayesian models, EpiEstim and EpiLPS.

There are also frequentist approaches for $\mathcal{R}_t$ estimation. Abry et al. (2020) proposed to regularize the smoothness of $\mathcal{R}_t$ regarding its temporal and spatial evolution. They considered a penalized regression with a second-order temporal regularization and a spatial regularization on $\mathcal{R}_t$ and with Poisson loss. Pascal et al. (2022) extended this procedure by introducing another penalty on outliers for robustness in. Pircalabelu (2023a) is a spline-based model relying on the assumption of exponential-family distributed incidences. Ho et al. (2023) estimates $\mathcal{R}_t$ while monitoring the time-varying level of overdispersion. There are other spline-based approaches such as Azmon et al. (2014); Gressani et al. (2021); Pircalabelu (2023b), autoregressive models with random effects (Jin et al., 2023) that are robust to low incidence cases, and generalized autoregressive moving average (GARMA) model (Hettinger et al., 2023) that are robust to measurement errors in incidence data.

We propose a retrospective effective reproduction number estimator called `RtEstim`that requires only incidence data. Our model makes the conditional Poisson assumption, similar to much of the prior work described above, but is empirically more robust to misspecification. This estimator is a convex optimization problem with Poisson loss and ℓ_1 penalty on the temporal evolution of $\log(\mathcal{R}_t)$ to impose smoothness over time. As a result `RtEstim` generates discrete splines, and the estimated curves appear to be piecewise polynomials of an order selected by the user. Importantly, The estimates are locally adaptive, meaning that different time ranges may posses heterogeneous smoothness.

Our approach is straightforward and requires little expertise in domain knowledge for implementation. We use a proximal Newton method to solve the convex optimization problem

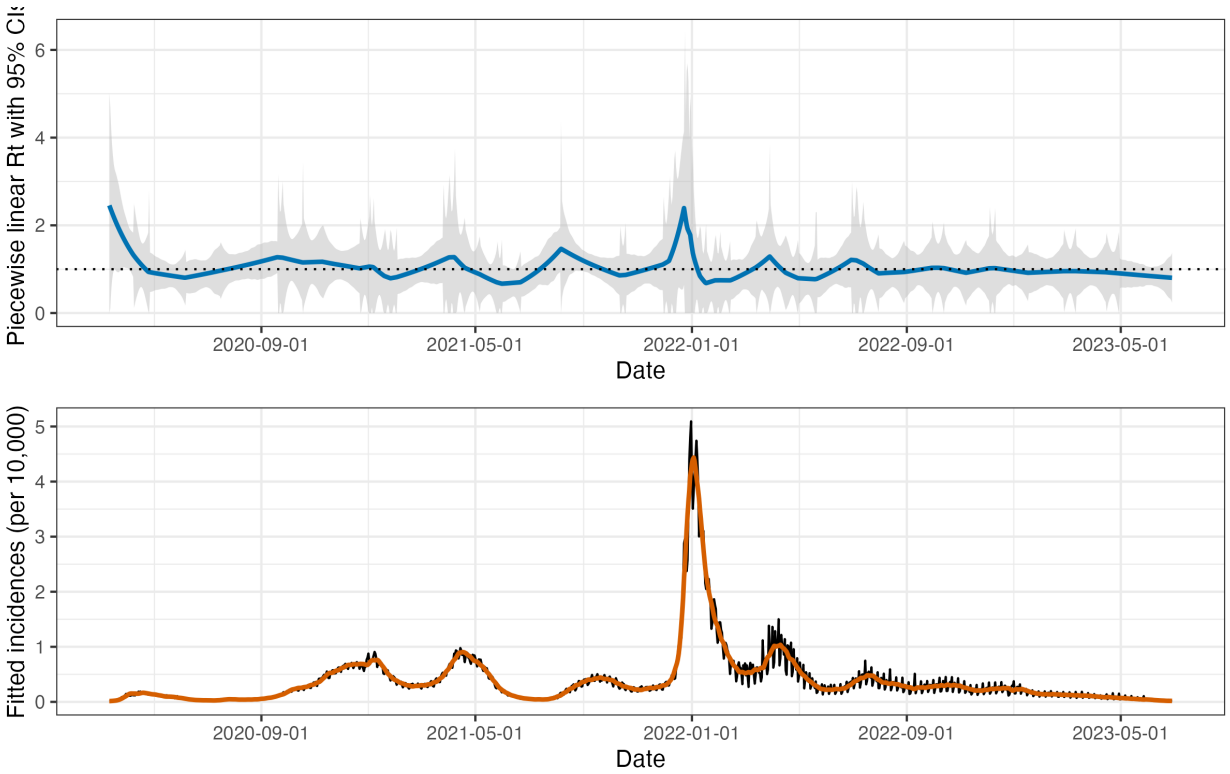

Figure 1: A demonstration of effective reproduction number estimation by `RtEstim` and the corresponding fitted incidence cases for the Covid-19 epidemic in British Columbia, Canada during a period from March 13, 2020 to June 28, 2023. The **blue** curve in the top panel is the estimated piecewise-linear $\mathcal{R}_t$ and the gray ribbon is the corresponding 95% confidence bands. The black curve in the bottom panel is the observed Covid-19 daily confirmed cases, and the **orange** curve is the fitted incidences corresponding to the estimated $\mathcal{R}_t$.

along with a number of computational tricks to produce estimates efficiently, typically in a matter of seconds even for long sequences of data. In a number of simulated experiments, we show empirically that our approach is more accurate than existing methods at estimating the true effective reproduction numbers.

The manuscript unfolds as follows. We first introduce the methodology of `RtEstim` including the usage of renewal equation, the development of Poisson trend filtering estimator, and the proximal Newton algorithm. We explain how this method can be interpreted from Bayesian perspective, connecting it to previous work in this context. We provide illustrative experiments comparing our estimator to `EpiEstim` and `EpiLPS`. We then apply our `RtEstim` on the Covid-19 pandemic incidence in British Columbia and the 1918 influenza pandemic in the United States. Finally, we conclude with a discussion on the advantages and limitations of our approach and as well as describe practical considerations for the effective reproduction number estimation.

2 Methods

2.1 Renewal model for incidence data

The effective reproduction number $\mathcal{R}(t)$ is defined to be the expected number of secondary infections at time t produced by a primary infection sometime in the past. To make this precise, denote the number of new infections at time t as $y(t)$. Then the total primary infectiousness can be written as $\eta(t) := \int_0^\infty p(i)y(t-i)\mathtt{d}i$, where $p(i)$ is the probability that a new secondary infection is the result primary infection which occurred i time units in the past. The reproduction number is then given as the value that equates

$$\mathbb{E}[y(t) \mid y(j),\ j < t] = \mathcal{R}(t)\eta(t) = \mathcal{R}(t) \int_0^\infty p(i)y(t-i)\mathtt{d}i, \tag{1}$$

otherwise known as the renewal equation. The period between primary and secondary infections is exactly the generation time of the disease, but given real data, observed at discrete times (say, daily) this delay distribution must be discretized into contiguous time intervals, say, $(0, 1], (1, 2], \ldots$, which results in the sequence $\{p_i\}_1^\infty$ corresponding to observations y_t and resulting in the discretized version of Equation (1),

$$\mathbb{E}[y_t \mid y_1, \ldots, y_{t-1}] = \mathcal{R}_t\eta_t = \mathcal{R}_t \sum_{i=0}^{\infty} p_i y_{t-i}. \tag{2}$$

Many approaches to estimating $\mathcal{R}_t$ rely on Equation (2) as motivation for their procedures, among them, `EpiEstim` (Cori et al., 2013) and `EpiFilter` (Parag, 2021).

In most cases, it is safe to assume that infectiousness disappears beyond τ timepoints ($p(i) = 0$ for $i > \tau$) so that the truncated integral of the generation interval distribution $\int_0^\tau p(i)\mathtt{d}i = 1$. Generation time, however, is usually unobservable and tricky to estimate, so common practice is to approximate it by the serial interval: the period between the symptom onsets of primary and secondary infections. If the infectiousness profile after symptom onset is independent of the incubation period (the period from the time of infection to the time of symptom onset), then this approximation is justifiable: the serial interval distribution and the generation interval distribution share the same mean. However, other properties may not be similarly shared, and, in general, the generation interval distribution is a convolution of the serial interval distribution with the distribution of the differance between independent draws from the delay distribution from infection to symptom onset. See, for example, Gostic et al. (2020) for a fuller discussion of the dangers of this approximation. Nonetheless, treating these as interchangable is common (Cori et al., 2013) and beyond the scope of this work.

Additionally, we assume that the generation interval (and, therefore, the serial interval), is constant over time t. That is, the probability $p(i)$ depends only on the gap between primary and secondary infections and not on the time t when the secondary infection occurs. For our methods, we will assume that the serial interval can be accurately estimated from auxilliary data (say by contact tracing, or previous epidemics) and we will take it as fixed, as is common in existing studies, e.g., Abry et al. (2020); Cori et al. (2013); Pascal et al. (2022).

The renewal equation in Equation (2) relates observable data streams (incident cases) occurring at different time points to the reproduction number given the serial interval. The fact that it depends only on the observed incidence counts makes it reasonable to estimate $\mathcal{R}_t$. However, this relationship obscures some difficulties in data collection. Diagnostic testing targets symptomatic individuals, omitting asymptomatic primary infections which can lead to future secondary infections. Testing practices, availability, and uptake can vary across space and time (Hitchings et al., 2021; Pitzer et al., 2021). Finally, incident cases as reported to public health are subject to delays due to laboratory confirmation, test turnaround times, and eventual submission to public health (Pellis et al., 2021). For these reasons, reported cases are lagging indicators of the course of the pandemic. Furthermore, they do not represent the actual number of new infections that occur on a given day, as indicated by exposure to the pathogen. The assumptions described above (constant serial interval distribution, homogenous mixing, similar susceptibility and social behaviours, etc.) are therefore consequential. That said, Equation (2) also provides some comfort about deviations from these assumptions. If y_t is scaled by a constant (in time) describing the reporting ratio, then it will cancel from both sides. Similar arguments mean that even if such a scaling varies in time, as long as it varies slowly relative to the set of p_i that are larger than 0, Equation (2) will be a reasonably accurate approximation, so that $\mathcal{R}_t$ can still be estimated well from reported incidence data. Finally, even a sudden change, say from c_1 for $i = 1, \ldots, t_1$ to c_2 for $i > t_1$ would only result in large errors for t in the neighbourhood of t_1 (where the size of this neighbourhood is again determined by the effective support of $\{p_i\}$). This robustness to certain types of data reporting issues provides some degree of comfort when depending on Equation (2) to calculate $\mathcal{R}_t$.

2.2 Poisson trend filtering estimator

We use the daily confirmed incident cases y_t on day t to estimate the observed infectious cases under the model that y_t given previous incident cases $y_{t-1}, \ldots, y_1$ and a constant serial

interval distribution follows a Poisson distribution with mean Λ_t. That is,

$$y_t \mid y_1, \ldots, y_{t-1} \sim \text{Poisson}(\Lambda_t), \text{ where } \Lambda_t = \mathcal{R}_t \sum_{i=0}^{t-1} p_i y_{t-i} = \mathcal{R}_t \eta_t.$$

Given a history of n confirmed incidence counts $\mathbf{y} = (y_1, \ldots, y_n)^\mathsf{T}$, our interest is to estimate $\mathcal{R}_t$. A natural approach is to maximize the likelihood, producing the MLE:

$$\begin{aligned} \widehat{\mathcal{R}} &= \underset{\mathcal{R} \in \mathbb{R}_+^n}{\text{argmax}}\ \mathbb{P}(\mathcal{R} \mid \mathbf{y},\ \mathbf{p}) = \underset{\mathcal{R} \in \mathbb{R}_+^n}{\text{argmax}} \prod_{t=1,\ldots,n} \frac{e^{-\mathcal{R}_t \eta_t} (\mathcal{R}_t \eta_t)^{y_t}}{y_t!} \\ &= \underset{\mathcal{R} \in \mathbb{R}_+^n}{\text{argmin}}\ \frac{1}{n} \sum_{t=1}^{n} \mathcal{R}_t \eta_t - y_t \log(\mathcal{R}_t \eta_t). \end{aligned} \tag{3}$$

This optimization problem, however, is easily seen to yield a one-to-one correspondence between the confirmed cases and the effective reproduction, i.e., $\widehat{\mathcal{R}}_t = y_t/\eta_t$, so that the estimated sequence $\widehat{\mathcal{R}}$ will have no significant graphical smoothness.

The MLE is an unbiased estimator of the true parameter $\mathcal{R}_t$, but unfortunately has high variance: changes in y_t result in proportional changes in $\widehat{\mathcal{R}}_t$. To avoid this behaviour, and to match the intuition that $\mathcal{R}_t \approx \mathcal{R}_{t-1}$, we advocate enforcing smoothness of the effective reproduction numbers. This requirement will decrease the variance, and hopefully lead to more accurate estimation of $\mathcal{R}$, as long as the smoothness assumption is reasonable. Smoothness assumptions are common (see e.g., Parag (2021) or Gostic et al. (2020)), but the *type* of smoothness assumed is critical. Cori et al. (2020) imposes smoothness indirectly by estimating $\mathcal{R}_t$ with moving windows of of past observations. The Kalman filter procedure of Parag (2021) would result in ℓ_2-smoothness ($\int_0^n (\widehat{\mathcal{R}}''(t))^2 \mathsf{d}t < C$ for some C), although the algorithm results in $\widehat{\mathcal{R}}$ taking values over a discrete grid. Pascal et al. (2022) produces piecewise-linear $\widehat{\mathcal{R}}_t$, which turns out to be a special case of our methodology. Smoother estimated curves will provide high-level information about the entire epidemic, obscuring small local changes in $\mathcal{R}(t)$, but may also remove the ability to detect large sudden changes, such as those resulting from lockdowns or other major containment policies.

We choose to implement smoothness by assuming that $\mathcal{R}(t)$ is a piecewise polynomial of arbitrary degree. We specifically consider discrete splines with various degrees of continuity. For example, 0^{th}-degree discrete splines are piecewise constant, the 1^{st}-degree curves are piecewise linear, and 2^{nd}-degree curves are piecewise quadratic. For $k \geq 1$, k^{th}-degree discrete splines are continuous and have continuous discrete differences up to degree $k-1$ at the knots. To achieve such smoothness, we regularize the size of changes between adjacent effective reproduction numbers. Because $\mathcal{R}_t > 0$, we explicitly penalize the divided differences (discrete

derivatives) of neighbouring values of $\log(\mathcal{R})_t$. To achieve this, we penalize the ℓ_1 norm of the divided differences, which introduces sparsity into the curvature, so that the estimates have heterogeneous smoothness in different subregions of the entire domain. It is a more realistic setting compared to homogeneous smoothness created by the squared ℓ_2 norm. Taking different orders of divided differences result in estimated effective reproduction numbers with different smoothness assumptions.

To enforce smoothness of $\hat{\mathcal{R}}_t$, we add a trend filtering penalty to Equation (4) (Kim et al., 2009; Sadhanala et al., 2022; Tibshirani, 2014; Tibshirani et al., 2022). Let $\theta := \log(\mathcal{R}) \in \mathbb{R}^n$, so that $\Lambda_t = \eta_t \exp(\theta_t)$, and $\log(\eta_t \mathcal{R}_t) = \log(\eta_t) + \theta_t$. For evenly spaced incident case data, we write our estimator as the solution to the optimization problem

$$\widehat{\mathcal{R}} = \exp(\widehat{\theta}) \quad \text{where} \quad \widehat{\theta} = \underset{\theta \in \mathbb{R}^n}{\operatorname{argmin}} \; \eta^{\mathsf{T}} \exp(\theta) - \mathbf{y}^{\mathsf{T}} \theta + \lambda \left\| D^{(k+1)} \theta \right\|_1, \tag{4}$$

where $\exp(\cdot)$ applies elementwise. Here, $D^{(k+1)} \in \mathbb{Z}^{(n-k-1)\times n}$ is the $(k+1)^{\text{th}}$ order divided difference matrix for any $0 \leq k < n-1$. $D^{(k+1)}$ is defined recursively as $D^{(k+1)} = D^{(1)} D^{(k)}$, where $D^{(1)} \in \{-1, 0, 1\}^{(n-k-1)\times(n-k)}$ is a banded matrix with diagonal band:

$$D^{(1)} = \begin{pmatrix} -1 & 1 & & & \\ & -1 & 1 & & \\ & & \ddots & \ddots & \\ & & & -1 & 1 \end{pmatrix}.$$

The tuning parameter λ balances data fidelity with desired smoothness. When $\lambda = 0$, the problem in Equation (4) reduces to the MLE in Equation (3). Larger tuning parameters privilege the regularization term and yield smoother estimates. Finally, there exists $\lambda_{\max}$ such that any $\lambda \geq \lambda_{\max}$ will result in $D^{(k+1)}\widehat{\theta} = 0$ and $\widehat{\theta}$ will be the Kullback-Leibler projection of $\mathbf{y}$ onto the null space of $D^{(k+1)}$.

For unevenly spaced incidence data, the spacing between neighboring parameters varies by the time between observations, and thus, the divided differences must be adjusted by the times that the observations occur. Given observation times $\mathbf{x} = (x_1, \ldots, x_n)^{\mathsf{T}}$, for $k \geq 1$, define a k^{th}-order diagonal matrix

$$X^{(k)} = \operatorname{diag}\left(\frac{k}{x_{k+1} - x_1}, \; \frac{k}{x_{k+2} - x_2}, \; \cdots, \; \frac{k}{x_n - x_{n-k}} \right).$$

Let $D^{(\mathbf{x},1)} := D^{(1)}$. Then for $k \geq 1$, the $(k+1)^{\text{th}}$-order divided difference matrix for unevenly

spaced data can be created recursively by

$$D^{(\mathbf{x},k+1)} := D^{(1)} X^{(k)} D^{(\mathbf{x},\ k)}.$$

Importantly, due to the penalty structure, this estimator is locally adaptive, meaning that it can potentially capture local changes such as the initiation of control measures. Abry et al. (2020); Pascal et al. (2022) considered only the 2nd-order divided difference of $\mathcal{R}_t$ rather than its logarithm. In comparison to their work, our estimator (1) allows for arbitrary degrees of temporal smoothness and (2) avoids the potential numerical issues of penalizing/estimating positive real values. Furthermore, as we will describe below, our procedure is computationally efficient for estimation over an entire sequence of penalty strengths λ and provides methods for choosing how smooth the final estimate should be.

2.3 Solving over a sequence of tuning parameters

We can solve the Poisson trend filtering estimator over an arbitrary sequence of λ that produces different levels of smoothness in the estimated curves. We consider a candidate set $\boldsymbol{\lambda} = \{\lambda_m\}_{m=1}^{M}$ of size M, which contains a strictly decreasing λ sequence.

Let $D := D^{(k+1)}$ for simplicity of the following notations. As $\lambda \to \infty$, the penalty term $\lambda \left\| D^{(k+1)}\theta \right\|_1$ dominants the PTF objective, so that minimizing the objective is asymptotically equivalent to minimizing the penalty term, which results in $\left\| D^{(k+1)}\theta \right\|_1 = 0$. In this case, the divided difference of θ with order $k+1$ is always 0, and thus θ is in the null space of D, i.e., $\theta \in \mathcal{N}(D)$. It happens for any λ beyond the threshold λ_{max}, so that λ_{max} is the minimum λ producing $\theta \in \mathcal{N}(D)$. It is of the following form:

$$\lambda_{max} = \left\| \left(D^{\dagger}\right)^{\mathsf{T}} (\eta - y) \right\|_{\infty},$$

where $D^{\dagger}$ is the generalized inverse of D with $D^{\dagger}D = I$. We may compute $\lambda_1 = \lambda_{max}$ through data, and then let the minimum $\lambda_M = \lambda_{min}$ be proportional to λ_{max} by a ratio $r \in (0, 1)$. Given the size $M \geq 3$, we generate λ values logarithmically equally spaced between λ_{min} and λ_{max}.

2.4 Choosing a final λ

We measure the model accuracy over the candidate set through a k-fold cross validation (CV) to choose the best tuning parameter. Specifically, we divide the all samples (except the earliest and latest case counts) roughly evenly and randomly into k folds, and build models on each sample set by leaving each fold out across all tuning parameters from the chosen candidate

set $\boldsymbol{\lambda}$ as in subsection 2.3. Leave-kth-out CV is a reasonable alternative, but its performance is not as satisfactory as randomly splitting the samples, since different folds generated in this way can be so similar to each other that hinder the variability of their performance on varying tuning parameters. Therefore, we prefer the k-fold CV in tuning parameter selection.

Model accuracy can be measured by multiple metrics including mean squared errors $\text{MSE}(\hat{y}, y) = \frac{1}{n} \|\hat{y} - y\|_2^2$, mean absolute errors $\text{MAE}(\hat{y}, y) = \frac{1}{n} \|\hat{y} - y\|_1$, and deviance in terms of Kullback-Leibler (KL) divergence between the estimated incidences $\hat{y}$ and the observed incidences y. We measure the deviance through the following function:

$$D_{\text{KL}}(y \parallel \hat{y}) = \frac{1}{n} \sum_{i=1}^{n} 2 \left(y_i \log(y_i) - y_i \log(\hat{y}_i) - y_i + \hat{y}_i \right).$$

Let $\log(y_i) := 0$, if $y_i = 0$.

We create a path algorithm to choose the best tuning parameter across the candidate set $\boldsymbol{\lambda}$. Model is fitted sequentially by visiting each component of $\boldsymbol{\lambda}$ in order. The estimates generated by model with a larger λ are input as the initial values for the next model with a smaller λ. By solving through a sequence of tuning parameters, we have a better chance to achieve a better trade-off between bias and variance, and accordingly a lower prediction risk, compared to many existing approaches, e.g., `EpiEstim` and `EpiLPS`, that do not support such tuning parameter selection. A larger candidate set requires more computational cost, but can potentially provide a better fit.

2.5 Approximate confidence bands

We also provide empirical confidence intervals of the estimators with approximate standard errors of an approximate estimator based on the results shown in Vaiter et al. (2017). Let $\hat{\mu}(y) := \eta \circ \hat{\mathcal{R}}(y) = \eta \circ \exp\left(\hat{\theta}(y)\right)$ be the approximate incidences estimator solving $\min_{\hat{\mu}(y)} F(\hat{\mu}(y), y) + J(\hat{\mu}(y))$, where $F(\hat{\mu}(y), y) := \sum_{i=1}^{n} -y_i \log(\hat{\mu}_i(y)) + \hat{\mu}_i(y)$ be the Poisson loss which is equivalent to the loss in Equation (4), and $J(\hat{\theta}(y)) := \lambda \|D^* \theta\|_2^2$ be the normal approximation of the original penalty, where D^* is a block diagonal matrix where each block is the divided difference matrix for the corresponding segment of the estimated $\mathcal{R}_t$. Based on Theorem 2 in Vaiter et al. (2017), the standard error of the approximate estimators with squared ℓ_2 penalty is

$$Var(\hat{\mu}(y)) = \left(\partial_{\hat{\mu}(y)}{}^2 F(\hat{\mu}(y), y) + \nabla^2 J(\hat{\theta}(y)) \right)^{\dagger} \tag{5}$$

$$= \left(I \left(\hat{\mu}(y) \right)^{-2} + \lambda \left(D^* \right)^{\intercal} D^* \right)^{\dagger}. \tag{6}$$

Since $\hat{\mu}(y) = \eta \circ \hat{\mathcal{R}}$, $Var(\hat{\mathcal{R}}_i) = Var(\hat{\mu}_i(y))/w_i^2$ for each $i = 1, \cdots, n$.

An approximate 95% confidence interval then can be written as $\hat{\mathcal{R}} \pm t_{0.975,n-df}\, s$, where s_i is the squared root of $Var(\hat{\mathcal{R}}_i)$ for each $i = 1, \cdots, n$ and df is the number of knots in the estimated $\mathcal{R}_t$ curves.

2.6 Bayesian perspective

Unlike many other methods for $\mathcal{R}_t$ estimation, our apporach is frequentist rather than Bayesian. Nonetheless, it can has a corresponding Bayesian interpretation: as a state-space model with Poisson observational noise, autoregressive transition equation of degree $k \geq 0$, e.g., $\theta_{t+1} = 2\theta_t - \theta_{t-1} + \varepsilon_{t+1}$ for $k = 1$, and Laplace transition noise $\varepsilon_{t+1} \sim \text{Laplace}(0,\ 1/\lambda)$. Compared to `EpiFilter` (Parag, 2021), another retrospective study of $\mathcal{R}_t$, we share same observational assumptions, but our approach has a different transition noise. `EpiFilter` estimates the posterior distribution of $\mathcal{R}_t$, and thus it can provide credible interval estimates as well. Our approach produces the maximum *a posteriori* estimate via an efficient convex optimization, omitting the need for MCMC sampling. But the associated confidence bands are approximated differently.

3 Results

Implementation of the our approach is provided in the `R` package `rtestim`. All experiments are run in `R` with version 4.3.1 on a MacBook with an Apple M1 Pro chip and RAM 32GB running under macOS Sonoma 14.0. The `R` packages used for simulation and real-data application are versions `EpiEstim_2.2-4`, `EpiLPS_1.2.0`, and `rtestim_0.0.4`.

3.1 Simulation settings

We simulate four scenarios of the time-varying effective reproduction numbers, intended to mimic different epidemics. The first two scenarios are simple cases that are rapidly controlled by intervention, where the graphical curves consist of one discontinuity and two segments. Scenario 1 has constant $\mathcal{R}_t$ before and after an intervention, while Scenario 2 grows exponentially, then decays. The other two scenarios are more complicated, where more waves in the epidemics are involved. Scenario 3 has four linear segments with three discontinuities, which reflect the effect of an intervention, resurgence to rapid transmission, and finally suppression of pandemic. Scenario 4 involves sinusoidal waves throughout the epidemic. The first three scenarios and the last scenario are motivated by (Gressani et al.,

2022; Parag, 2021) respectively. We name the four scenarios as (1) 2-segment constant, (2) 2-segment exponential curve, (3) 4-segment linear, and (4) periodic respectively.

In all cases, the times of observation are regular, and consider epidemics of length $n = 300$. Specifically, in Scenario 1, $\mathcal{R}_t = 2, 0.8$ before and after $t = 70$. In Scenario 2, $\mathcal{R}_t$ increases and decreases exponentially with rates $0.015, 0.005$ pre and post $t = 50$. In Scenario 3, $\mathcal{R}_t$ reduces from 2.5 to 2 linearly between $t \in [1, 60]$, falls to 0.8 at $t = 61$ and goes linearly down to 0.6 until $t = 110$, resurges to 1.7 at $t = 111$ and grows linearly back to 2 until $t = 150$, and then drops to 0.9 at $t = 151$ and descends to 0.5 until the end. In Scenario 4, $\mathcal{R}_t$ is realization of the continuous, periodic curve generated by the function

$$\mathcal{R}(t) = 0.2\left(\left(\sin(\frac{\pi t}{12}) + 1\right) + \left(2\sin\left(\frac{\pi t}{6}\right) + 2\right) + \left(3\sin(\frac{\pi t}{1.2}) + 3\right)\right)$$

at equally spaced points $t \in [0, 10]$. These settings are illustrated in the left column of Figure 2.

We assume that the serial interval follows Gamma distribution with fixed shapes and scales $(3, 3)$, $(2.5, 2.5)$, $(3.5, 3.5)$ and $(3.5, 3.5)$ for Scenarios 1–4 respectively. We consider all epidemics starting from $y_1 = 2$ cases and generating until timepoints $t = 300$. We compute the expected incidence Λ_t using the renewal equation, and generate the incidence samples from the Poisson distribution $y_t \sim \text{Pois}(\Lambda_t)$. To verify the performance of our model under the violation of this distributional assumption of incidence, we also generate incidence samples using the negative Binomial distribution with dispersion size 5, i.e., $y_t \sim \text{NB}(\Lambda_t, \text{size} = 5)$. We generate 50 random samples for each setting of experiments, resulting in 400 total experiments. An example of each effective reproduction number scenario with a single corresponding Poisson and negative Binomial sample incidence sequence are displayed in Figure 2.

We compare `RtEstim` to `EpiEstim` and `EpiLPS`. Unfortunately, `EpiFilter` frequently fails to converge due to the large case counts in many simulations. `EpiEstim` estimates the posterior distribution of effective reproduction numbers given a Gamma prior and Poisson distributed incidences. It estimates the reproduction number over a sliding window, assuming the reproduction number is constant during the specific time window. A longer sliding window averages out more fluctuations, leading to smoother estimates, whereas, a shorter sliding window is more responsive to sudden spikes or declines. We tried the default, a weekly sliding window, as well as a monthly window. However, since neither considerably outperform the other across all scenarios, we defer the monthly case to the Appendix. `EpiLPS` is another Bayesian approach that estimates P-splines coupled with Laplace approximations of the conditional posterior based on the negative Binomial likelihood. For `RtEstim` on the four scenarios respectively, we estimate (1) piecewise constant $k = 0$, (2) piecewise linear & cubic

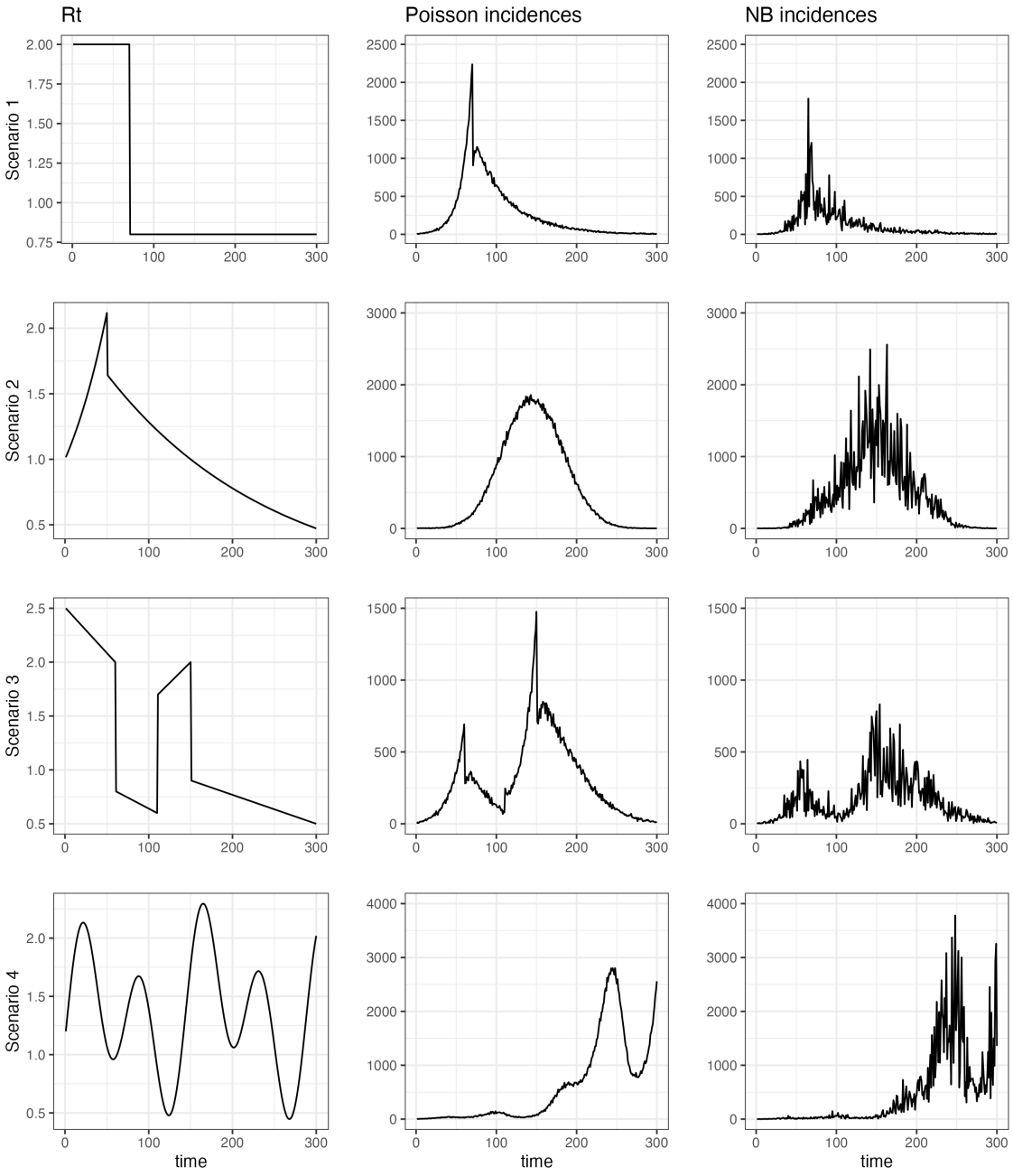

Figure 2: The effective reproduction numbers (left column) and corresponding sample incident cases drawn from a Poisson (middle column) or negative Binomial (right column) distribution. The rows correspond to the four $\mathcal{R}_t$ settings.

$k = 1, 3$, (3) piecewise linear $k = 1$ and (4) piecewise cubic polynomials $k = 3$. In each case, we examine a grid of 50 λs, selecting the best using cross validation. For all models and problems, we use the generation interval distribution used to create the data.

To measure estimation accuracy, we compare $\widehat{\mathcal{R}}$ to $\mathcal{R}$ using the KL divergence: a standard metric that measures the distance between two probability distributions. Since $\mathcal{R}_t$ can be regarded as the expectation of Poisson distribution, we use the mean KL divergence for Poisson distributions (averaged across all coordinates) to measure the accuracy of the $\mathcal{R}_t$ estimates, i.e., $\overline{D}_{KL}(\mathcal{R} \parallel \widehat{\mathcal{R}}) = \frac{1}{n} D_{KL}(\mathcal{R} \parallel \widehat{\mathcal{R}})$, where

$$D_{KL}(\mathcal{R} \parallel \widehat{\mathcal{R}}) = \sum_{t=1}^{n} w_t \left(\mathcal{R}_t \log \left(\frac{\mathcal{R}_t}{\widehat{\mathcal{R}}_t} \right) + \widehat{\mathcal{R}}_t - \mathcal{R}_t \right),$$

where $\mathcal{R} = \{\mathcal{R}_t\}_{t=1}^n$ and $w_t = \eta_t / \sum_t \eta_t$ is the rescaled total infectiousness. To fairly compare across methods, we drop the estimates during the first week because estimates from `EpiEstim` do not begin until $t = 8$ (using a weekly window). KL divergence is more appropriate for measuring accuracy because it connects directly to the Poisson likelihood used to generate the data, whereas standard measures like the mean-squared error correspond to Gaussian data. This has the effect of increasing the relative cost of mistakes when Λ_t is small.

For a better interpretation of model performance, we introduce a baseline performance of $\mathcal{R}^*$, which is the sliding average of past true $\mathcal{R}$. We take the sliding window to be a week, which is similar as the setting of the estimators used in the experiments. Specifically, $\mathcal{R}_t^*$ at time $t > 7$ is set to be the average of $\mathcal{R}_{t-7}^*, \cdots, \mathcal{R}_{t-1}^*$. The baseline $\mathcal{R}_t^*$ performance represents the "close-to-best" performance that we can achieve given the knowledge of $\mathcal{R}$. All KL divergences between $\widehat{\mathcal{R}}$ and $\mathcal{R}$ are divided by the corresponding baseline, i.e., KL divergence between $\mathcal{R}_t^*$ and $\mathcal{R}$, to conduct the KL ratio $r = \frac{D_{KL}(\mathcal{R} \| \widehat{\mathcal{R}})}{D_{KL}(\mathcal{R} \| \mathcal{R}^*)}$. If $r < 1$, $\widehat{\mathcal{R}}$ outperforms the baseline; the larger the ratio is, the worse the performance of $\widehat{\mathcal{R}}$ is. Other details of the experimental settings are deferred to the Appendix.

3.2 Simulation results

`RtEstim` overall outperforms `EpiEstim` and `EpiLPS` in the experimental study. Figure 3 visualizes the KL divergence ratio across the three models. Under both Poisson and negative Binomial distributions, `RtEstim` is easily the most accurate across Scenarios 1, 3, and 4: the median of KL divergence ratio is much lower and the boxes frequently fail to overlap indicating that better performance than the other two methods across all 50 simulations. The advantage is less for the negative Binomial case compared to the Poisson case, but still obvious. `EpiLPS` tends to dominate in Scenario 2 as the boxes of KL ratios are lower than those of the other two

methods for both incidence distributions, but `EpiLPS` has large outliers for negative Binomial incidences cases. We will examine a single realization of each experiment to investigate these global conclusions in more datail.

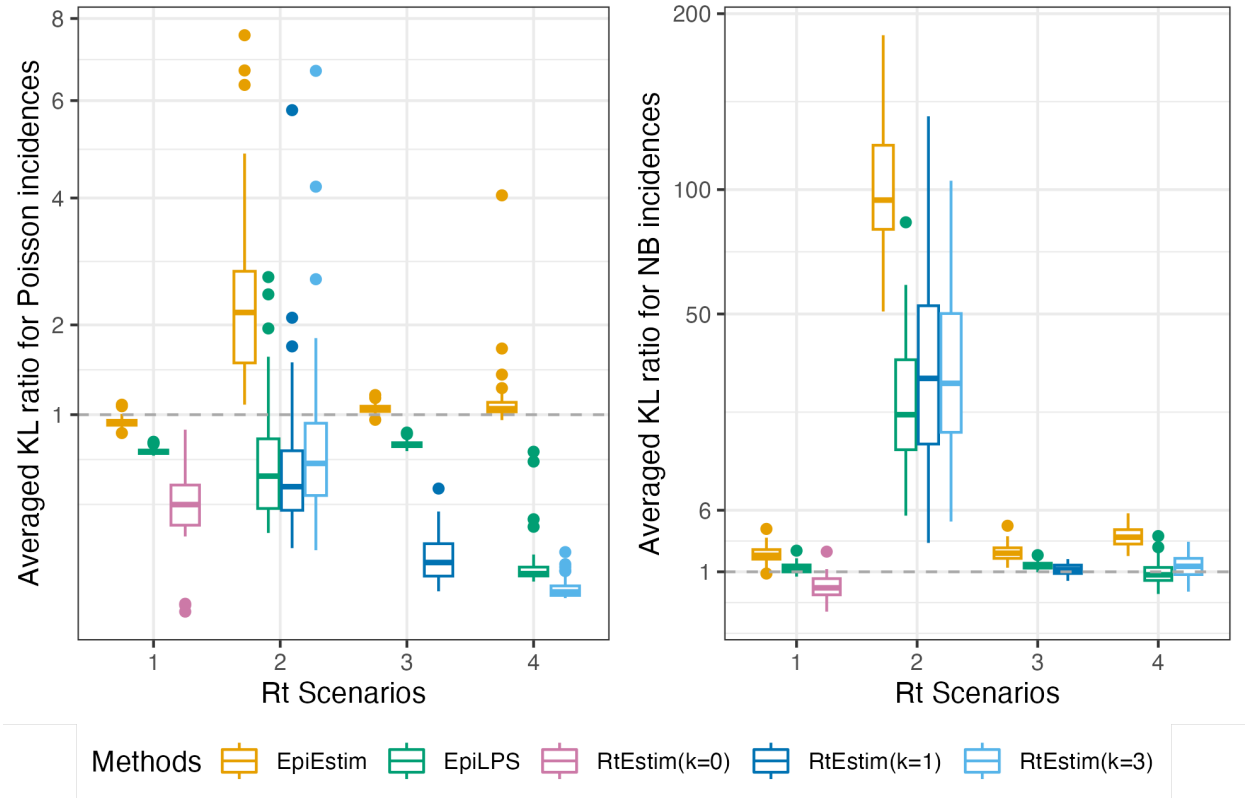

Figure 3: Boxplot of KL divergence ratios of KL divergence between the estimated $\hat{\mathcal{R}}_t$ and the true $\mathcal{R}_t$ over the KL divergence between the baseline $\mathcal{R}_t^*$ and true $\mathcal{R}_t$ across all methods across 50 random samples for each approach given Poisson incidences *(left panel)* and negative Binomial incidences *(right panel)* respectively. Both y-axes are on a squared root scale for a better visualization. A few outliers of `EpiEstim` and `EpiLPS` for Scenario 2 given both Poisson and negative Binomial incidences are excluded. Full visualization is deferred to the supplementary document. A few `RtEstim` models for Scenario 2 run expired, and thus, are excluded here.

Figure 4 shows 1 realization for the estimated reproduction numbers under the Poisson generative model for all 4 scenarios. Compared to `EpiEstim` and `EpiLPS`, which have rather severe difficulties at the beginning of the time series, `RtEstim` estimates are more accurate—they nearly overlap with the true values—without suffering from the edge problem. Scenario 2 is a difficult problem for all methods: the sharp increase at the end of the stage of exponential growth is difficult to capture. Although the truth is piecewise exponential and likely best represented with a piecewise cubic curve, the actual curvature is so gentle that linear estimation ($k = 1$) appears potentially reasonable. We, therefore, fit piecewise linear and cubic $\hat{\mathcal{R}}_t$ curves

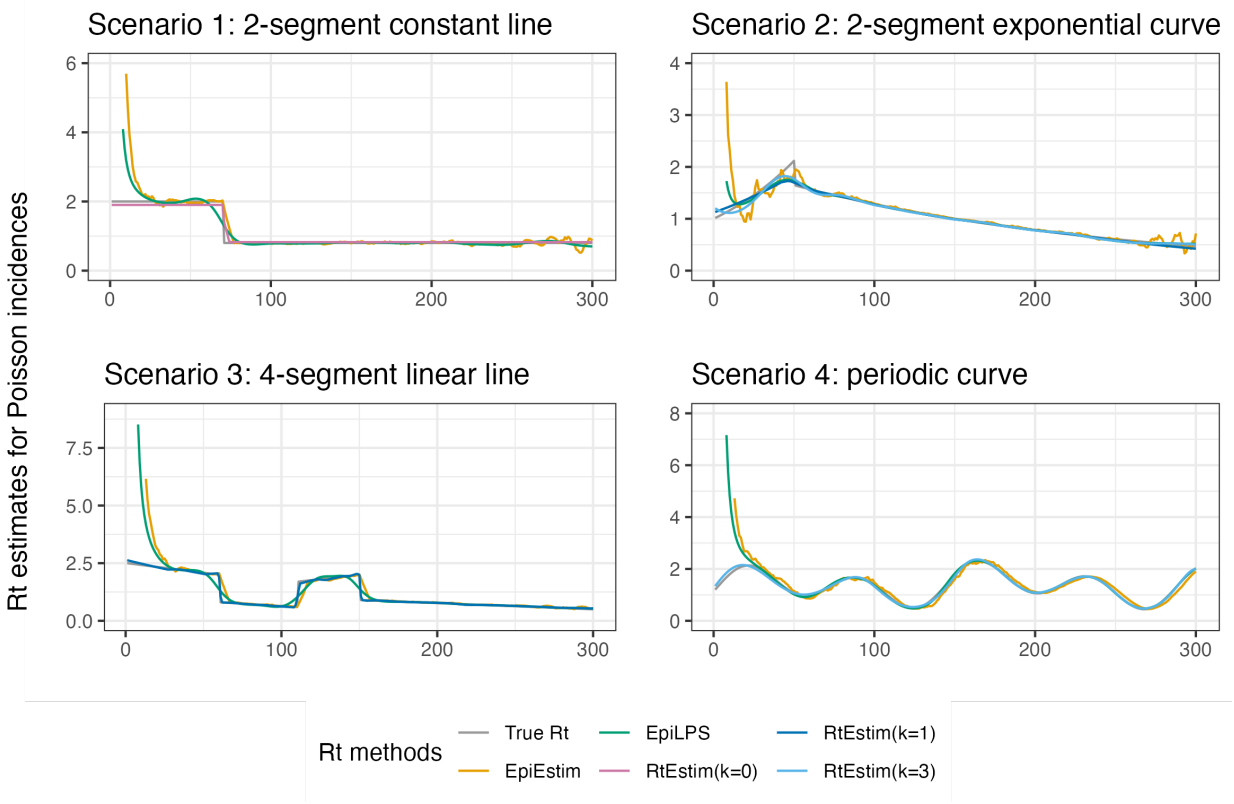

Figure 4: Example of effective reproduction number estimation for Poisson incidences.

using `RtEstim` for Scenario 2 to evaluate model misspecification. However, both cases have difficulty recovering the acute rise in the growth phase. An explanation of such failure is that the model imposes continuity at the changepoint, which hinders the estimates from fitting the two discontinuous phases. Scenario 1 is the simplest case with only one knot and two constant segments. Besides the edge problem, `EpiEstim` and `EpiLPS` produce "smooth" estimated curves that are continuous at the changepoint, which results in large mistakes in that neighbourhood. Since the piecewise constant `RtEstim` estimator does force any smoothness in $\mathcal{R}_t$, it easily captures the sharp decrease change.

To investigate the performance under the violation of the Poisson distributional assumption (of both `RtEstim` and `EpiEstim`), we also examine estimation accuracy with negative Binomial data. Figure 5 displays a realization, analogous to the previous case, for all methods and scenarios. `RtEstim` has more difficulty relative to the Poisson incidence setting, especially at the beginning of the outbreak. This is most pronounced in Scenario 4, where `RtEstim` is overly smooth, except in the last wave. In Scenario 2, `RtEstim` successfully captures the changepoint, but suffers from the same problem as in the Poisson setting. In Scenario 3, the piecewise linear `RtEstim` recovers the curvature of $\mathcal{R}_t$ well, but is less accurate than in the Poisson incidence cases.

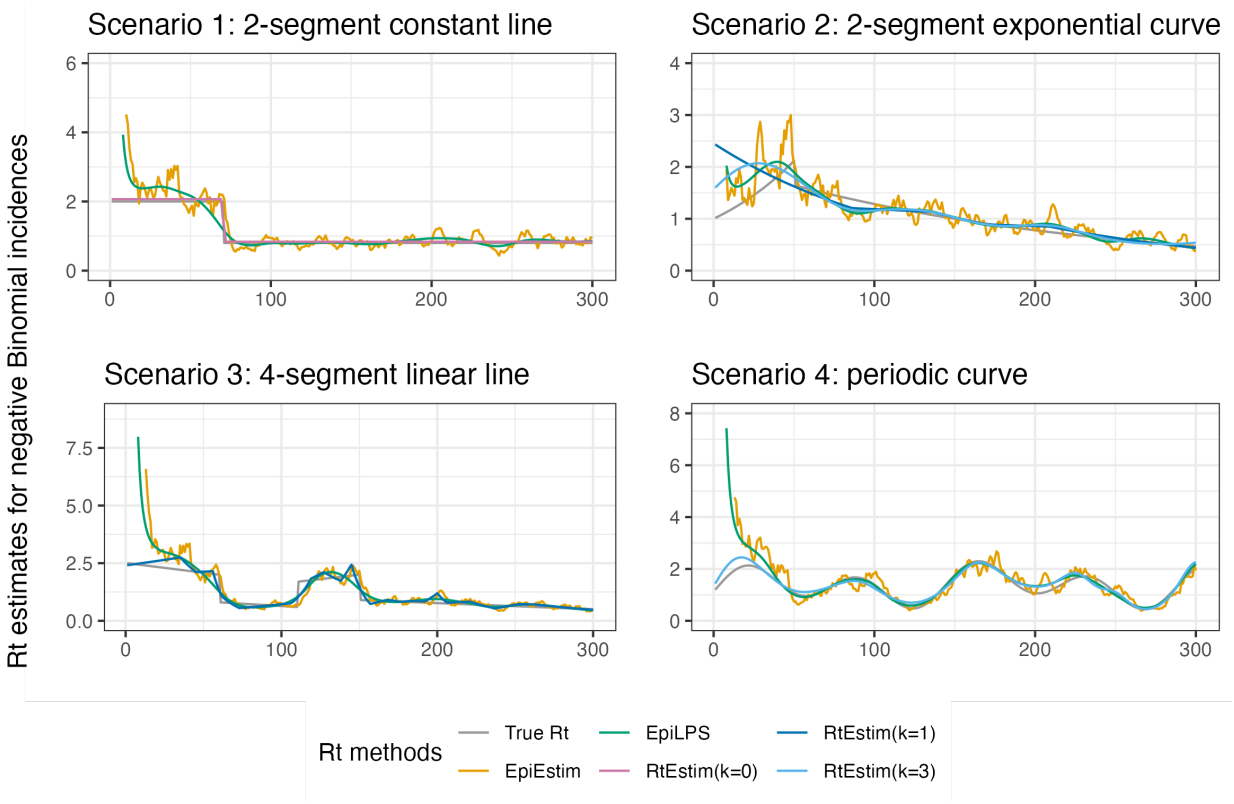

Figure 5: Example of effective reproduction number estimation for negative Binomial incidences.

Finally, it is important to provide a brief comparison of the running times of three models across the 8 experimental settings. We find that almost all models across all experiments complete within 10 seconds. `RtEstim` generally takes the longest, likely due to a relatively large candidate set—50 values of λ and 3 folds of cross validation—while other models run only a single time for a fixed setting of hyperparameters per experiment. Additional results on timing comparisons are deferred to the supplementary document.

3.3 Real-data results: Covid-19 incident cases in British Columbia

We implement `RtEstim` on Covid-19 incident confirmed cases in British Columbia (B.C.) as reported on May 18, 2023 (visualized in Figure 6) by the B.C. Centre for Disease Control. The reported incident cases provide a snapshot of how testing recommendations and practices have changed over the three years. We use the gamma distribution with shape 2.5 and scale 2.5 to approximate the serial interval function, which is empirically reasonable, since they are close to the parameters in a recent study (Lehtinen et al., 2021), which summarizes estimated parameters of the serial interval distributions of SARS-CoV-2 by different approaches.

Considering the first, second, and third polynomial degrees, the estimated effective

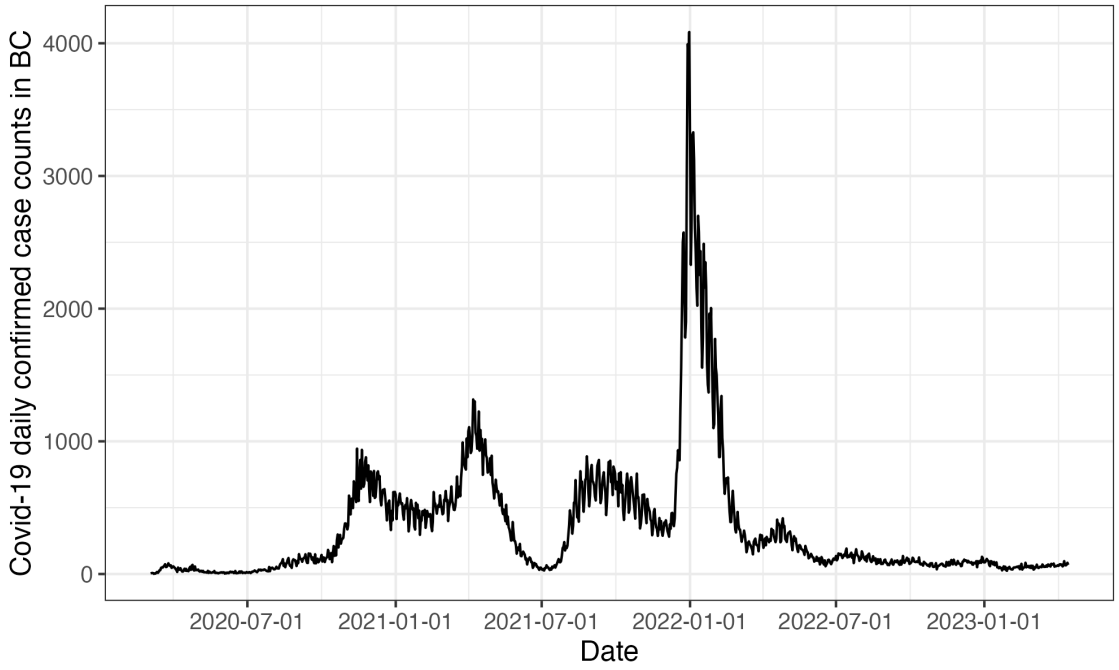

Figure 6: Covid-19 daily confirmed incident cases between March 1st, 2020 and April 15th, 2023 in British Columbia, Canada.

reproduction numbers of Covid-19 in British Columbia (illustrated in Figure 7) are always less than 3 except at the very early stage, which means that one distinct infected individuals on average infects less than three other individuals in the population. Examining three different settings for k, the temporal evolution of $\widehat{\mathcal{R}}$ (across all regularization levels λ) are similar near the highest peak around the end of 2021 before dropping shortly thereafter. Throughout the estimated curves, the peaks and troughs of the reproduction numbers precede the growth and decay cycles of confirmed cases, as expected. We also visualize 95% confidence bands for the point estimates at the smallest one of the "optimal" tuning parameters with lowest CV scores in Figure 7.

The estimated reproduction numbers are relatively unstable before April 1st, 2022. The highest peak coincides with the emergence and global spread of the Omicron variant. The estimated reproduction numbers fall below 1 during two time periods—roughly from April 1st, 2021 to July 1st, 2021 and from January 1st, 2022 to April 1st, 2022. The first trough coincides with the introduction of Covid-19 vaccines in British Columbia. The second trough, shortly after the greatest peak may be due to variety of factors resulting in the depletion of the susceptible population such as increased self-isolation in response to the peak and media and immunity incurred via recent infection. Since around April 1st, 2022, estimated reproduction numbers have remained relatively stable stable (fluctuating around 1) corresponding to low

reported cases (though reporting behaviours have also changed significantly since the Omicron wave).

3.4 Real-data results: Pandemic influenza in Baltimore, Maryland, 1918

We also apply `RtEstim` to daily reported influenza cases in Baltimore, Maryland occurring during the world-wide pandemic of 1918 from September to November. The dataset (shown in Figure 8) is included in the `EpiEstimR` package. The 1918 influenza outbreak, caused by the H1N1 influenza A virus, was an unprecedentedly deadly, infecting almost one-third of the population across the world (Taubenberger and Morens, 2006). In Figure 9, the CV-tuned piecewise cubic estimates best capture the growth at the beginning of the pandemic. It suggests that the pandemic grew rapidly over the first 30 before declining below 1 when the after 50 days. However, it also suggests an increase toward the end of the period. With the currently available dataset, it is hard to tell if there is a next wave or a steady decline ahead. The CV-tuned piecewise constant and linear estimates in Figure 9 both suggest a steady decline. It is supported by a couple of arguments. The influenza incidences reduce to 0 in the end. The $\mathcal{R}$ estimates of `EpiEstim` with 1-week, 2-week and 4-week sliding windows in Cori et al. (2013) are all lower than the threshold 1 in their right tails.

4 Discussion

The `RtEstim` methodology provides a locally adaptive estimator using Poisson trend filtering on univariate data. It captures the heterogeneous smoothness of effective reproduction numbers given observed incidence data rather than resulting in global smoothness. This is a nonparametric regression model which can be written as a convex optimization (minimization) problem. Minimizing the distance (averaged KL divergence per coordinate) between the estimators and (functions of) observations guarantees data fidelity while the divided differences between pairs of neighbouring parameters imposes smoothness. The ℓ_1-regularization results in sparsity of the divided differences, which leads to heterogeneous smoothness within certain periods of time.

The property of local adaptivity (heterogenous smoothness) is useful to automatically distinguish, for example, seasonal outbreaks from outbreaks driven by other factors (behavioural changes, foreign introduction, etc.). Given a well-chosen polynomial degree, for example, the growth rates can be quickly detected, alerting public health to implement policy changes. The effective reproduction numbers can be estimated retrospectively to examine the efficacy

of such policies, whether they result in $\mathcal{R}_t$ falling below 1 or the speed of their effects. The smoothness of $\mathcal{R}_t$ curves (including the polynomial degrees and tuning parameters) should be chosen based on the purpose of the study in practice, e.g., epidemic forecasting may require a more wiggly curve that contains more fluctuation information, while retrospective studies that solely target on understanding of the pandemic may prefer a smoother curve with less important information smoothed out.

Our method `RtEstim` provides a natural way to deal with missing data, for example, on weekends and holidays or due to changes in reporting frequency. While solving the convex optimization problem, the edge lengths of the line graphs are adjusted, correctly penalizing the distance between irregularly spaced data. Computing the total primary infectiousness is also easily generalized to irregular reporting by modifying the discretization of the serial interval distribution. Additionally, the because the ℓ_1-penalty introduces sparsity (operating like a median rather than a mean), this procedure is relatively insensitive to outliers compared to ℓ_2 regularization.

There are a number of limitations that may influence the quality of $\mathcal{R}_t$ estimation. While our model is generic for incidence data, rather than tailored to any specific disease, it does assume that the generation interval is short relative to the period of data collection. More specialized methodologies would be required for diseases with long incubation periods such as HIV or Hepatitis. Our approach, does not explicitly model imported cases, nor distinguish between subpopulations that may have different mixing behaviour. While the Poisson distribution is common, it does not handle overdispersion (observation variance larger than the mean). The negative binomial distribution is a good alternative, but more difficult to estimate in this context. As described in the introduction, justifying the expression for $\mathcal{R}$ assumes that a relatively constant proportion of true infections are reported. However, if this proportion varies with time (say, due to change in surveillance practices and testing recommendations), the estimates may be biased over this window. A good example is that in early January 2021, during the height of the Omicron wave, British Columbia moved from testing all symptomatic individuals to testing only those in at-risk groups. The result was a sudden change that would render $\mathcal{R}_t$ estimates on either side of this time point incommensurable.

As currently implemented, `RtEstim` uses a fixed serial interval throughout the period of study, but as factors such as population immunity vary, the serial interval may vary as well (Nash et al., 2023). Another issue relates to the equating serial and generation intervals (also mentioned above). The serial interval distribution is generally wider than that of the generation interval, because the serial interval involves the convolution of two distributions, and is unlikely to actually follow a named distribution like Gamma, though it may be reasonably

well approximated by one. Our implementation allows for an arbitrary distribution to be used, but requires the user to specify the discretization explicitly, requiring more nuanced knowledge than is typically available. Pushing this analysis further, to accommodate other types of incidence data (hospitalizations or deaths), a modified interval distribution would be necessary, and further assumptions would be required as well. Or else, one would first need to deconvolve deaths to infection onset before using our software.

Besides all the advantages and limitations of the methodology discussed above, our `RtEstim` estimator can be implemented easily through a lightweight `R` package `rtestim` and computed efficiently through the numerical algorithm, proximal Newton method developed in `C++`, especially for large-scale data. With accessible incidence cases, prespecified serial interval distribution, and chosen polynomial degrees, `RtEstim` is able to produce accurate estimation of effective reproduction numbers and provide tuning parameter selection through a path algorithm.

References

Sam Abbott, Joel Hellewell, Katharine Sherratt, Katelyn Gostic, Joe Hickson, Hamada S. Badr, Michael DeWitt, Robin Thompson, EpiForecasts, and Sebastian Funk. *EpiNow2: Estimate Real-Time Case Counts and Time-Varying Epidemiological Parameters*, 2020a.

Sam Abbott, Joel Hellewell, Robin N Thompson, Katharine Sherratt, Hamish P Gibbs, Nikos I Bosse, James D Munday, Sophie Meakin, Emma L Doughty, June Young Chun, et al. Estimating the time-varying reproduction number of sars-cov-2 using national and subnational case counts. *Wellcome Open Research*, 5(112):112, 2020b.

Patrice Abry, Nelly Pustelnik, Stéphane Roux, Pablo Jensen, Patrick Flandrin, Rémi Gribonval, Charles-Gérard Lucas, Éric Guichard, Pierre Borgnat, and Nicolas Garnier. Spatial and temporal regularization to estimate covid-19 reproduction number r (t): Promoting piecewise smoothness via convex optimization. *Plos one*, 15(8):e0237901, 2020.

Amin Azmon, Christel Faes, and Niel Hens. On the estimation of the reproduction number based on misreported epidemic data. *Statistics in medicine*, 33(7):1176–1192, 2014.

Anne Cori, Neil M Ferguson, Christophe Fraser, and Simon Cauchemez. A new framework and software to estimate time-varying reproduction numbers during epidemics. *American journal of epidemiology*, 178(9):1505–1512, 2013.

Anne Cori, Simon Cauchemez, Neil M Ferguson, Christophe Fraser, Elisabeth Dahlqwist,

P Alex Demarsh, Thibaut Jombart, Zhian N Kamvar, Justin Lessler, Shikun Li, et al. Package 'epiestim'. *CRAN: Vienna Austria*, 2020.

Katelyn M Gostic, Lauren McGough, Edward B Baskerville, Sam Abbott, Keya Joshi, Christine Tedijanto, Rebecca Kahn, Rene Niehus, James A Hay, Pablo M De Salazar, et al. Practical considerations for measuring the effective reproductive number, r_t. *PLoS computational biology*, 16(12):e1008409, 2020.

Oswaldo Gressani, Christel Faes, and Niel Hens. An approximate bayesian approach for estimation of the reproduction number under misreported epidemic data. *MedRxiv*, pages 2021–05, 2021.

Oswaldo Gressani, Jacco Wallinga, Christian L Althaus, Niel Hens, and Christel Faes. Epilps: A fast and flexible bayesian tool for estimation of the time-varying reproduction number. *PLoS computational biology*, 18(10):e1010618, 2022.

Gary Hettinger, David Rubin, and Jing Huang. Estimating the instantaneous reproduction number with imperfect data: A method to account for case-reporting variation and serial interval uncertainty. *arXiv preprint arXiv:2302.12078*, 2023.

Matt DT Hitchings, Natalie E Dean, Bernardo García-Carreras, Thomas J Hladish, Angkana T Huang, Bingyi Yang, and Derek AT Cummings. The usefulness of the test-positive proportion of severe acute respiratory syndrome coronavirus 2 as a surveillance tool. *American journal of epidemiology*, 190(7):1396–1405, 2021.

Faith Ho, Kris V Parag, Dillon C Adam, Eric HY Lau, Benjamin J Cowling, and Tim K Tsang. Accounting for the potential of overdispersion in estimation of the time-varying reproduction number. *Epidemiology*, 34(2):201–205, 2023.

Shihui Jin, Borame Lee Dickens, Jue Tao Lim, and Alex R Cook. Epimix: A novel method to estimate effective reproduction number. *Infectious Disease Modelling*, 2023.

Seung-Jean Kim, Kwangmoo Koh, Stephen Boyd, and Dimitry Gorinevsky. ℓ_1 trend filtering. *SIAM review*, 51(2):339–360, 2009.

Sonja Lehtinen, Peter Ashcroft, and Sebastian Bonhoeffer. On the relationship between serial interval, infectiousness profile and generation time. *Journal of the Royal Society Interface*, 18(174):20200756, 2021.

Adrian Lison, Sam Abbott, Jana Huisman, and Tanja Stadler. Generative bayesian modeling to nowcast the effective reproduction number from line list data with missing symptom onset dates. *arXiv preprint arXiv:2308.13262*, 2023.

Rebecca K Nash, Samir Bhatt, Anne Cori, and Pierre Nouvellet. Estimating the epidemic reproduction number from temporally aggregated incidence data: A statistical modelling approach and software tool. *PLOS Computational Biology*, 19(8):e1011439, 2023.

Kris V Parag. Improved estimation of time-varying reproduction numbers at low case incidence and between epidemic waves. *PLoS Computational Biology*, 17(9):e1009347, 2021.

Barbara Pascal, Patrice Abry, Nelly Pustelnik, Stéphane Roux, Rémi Gribonval, and Patrick Flandrin. Nonsmooth convex optimization to estimate the covid-19 reproduction number space-time evolution with robustness against low quality data. *IEEE Transactions on Signal Processing*, 70:2859–2868, 2022.

Lorenzo Pellis, Francesca Scarabel, Helena B Stage, Christopher E Overton, Lauren HK Chappell, Elizabeth Fearon, Emma Bennett, Katrina A Lythgoe, Thomas A House, Ian Hall, et al. Challenges in control of covid-19: short doubling time and long delay to effect of interventions. *Philosophical Transactions of the Royal Society B*, 376(1829):20200264, 2021.

Eugen Pircalabelu. A spline-based time-varying reproduction number for modelling epidemiological outbreaks. *Journal of the Royal Statistical Society Series C: Applied Statistics*, page qlad027, 2023a.

Eugen Pircalabelu. A spline-based time-varying reproduction number for modelling epidemiological outbreaks. *Journal of the Royal Statistical Society Series C: Applied Statistics*, page qlad027, 2023b.

Virginia E Pitzer, Melanie Chitwood, Joshua Havumaki, Nicolas A Menzies, Stephanie Perniciaro, Joshua L Warren, Daniel M Weinberger, and Ted Cohen. The impact of changes in diagnostic testing practices on estimates of covid-19 transmission in the united states. *American Journal of Epidemiology*, 190(9):1908–1917, 2021.

Veeranjaneyulu Sadhanala, Robert Bassett, James Sharpnack, and Daniel J McDonald. Exponential family trend filtering on lattices. *arXiv preprint arXiv:2209.09175*, 2022.

Jeffery K Taubenberger and David M Morens. 1918 influenza: the mother of all pandemics. *Revista Biomedica*, 17(1):69–79, 2006.

Robin N Thompson, Jake E Stockwin, Rolina D van Gaalen, Jonny A Polonsky, Zhian N Kamvar, P Alex Demarsh, Elisabeth Dahlqwist, Siyang Li, Eve Miguel, Thibaut Jombart, et al. Improved inference of time-varying reproduction numbers during infectious disease outbreaks. *Epidemics*, 29:100356, 2019.

Ryan J Tibshirani. Adaptive piecewise polynomial estimation via trend filtering. *The Annals of Statistics*, 42(1):285–323, 2014.

Ryan J Tibshirani et al. Divided differences, falling factorials, and discrete splines: Another look at trend filtering and related problems. *Foundations and Trends® in Machine Learning*, 15(6):694–846, 2022.

Cristiano Trevisin, Enrico Bertuzzo, Damiano Pasetto, Lorenzo Mari, Stefano Miccoli, Renato Casagrandi, Marino Gatto, and Andrea Rinaldo. Spatially explicit effective reproduction numbers from incidence and mobility data. *Proceedings of the National Academy of Sciences*, 120(20):e2219816120, 2023.

Samuel Vaiter, Charles Deledalle, Jalal Fadili, Gabriel Peyré, and Charles Dossal. The degrees of freedom of partly smooth regularizers. *Annals of the Institute of Statistical Mathematics*, 69:791–832, 2017.

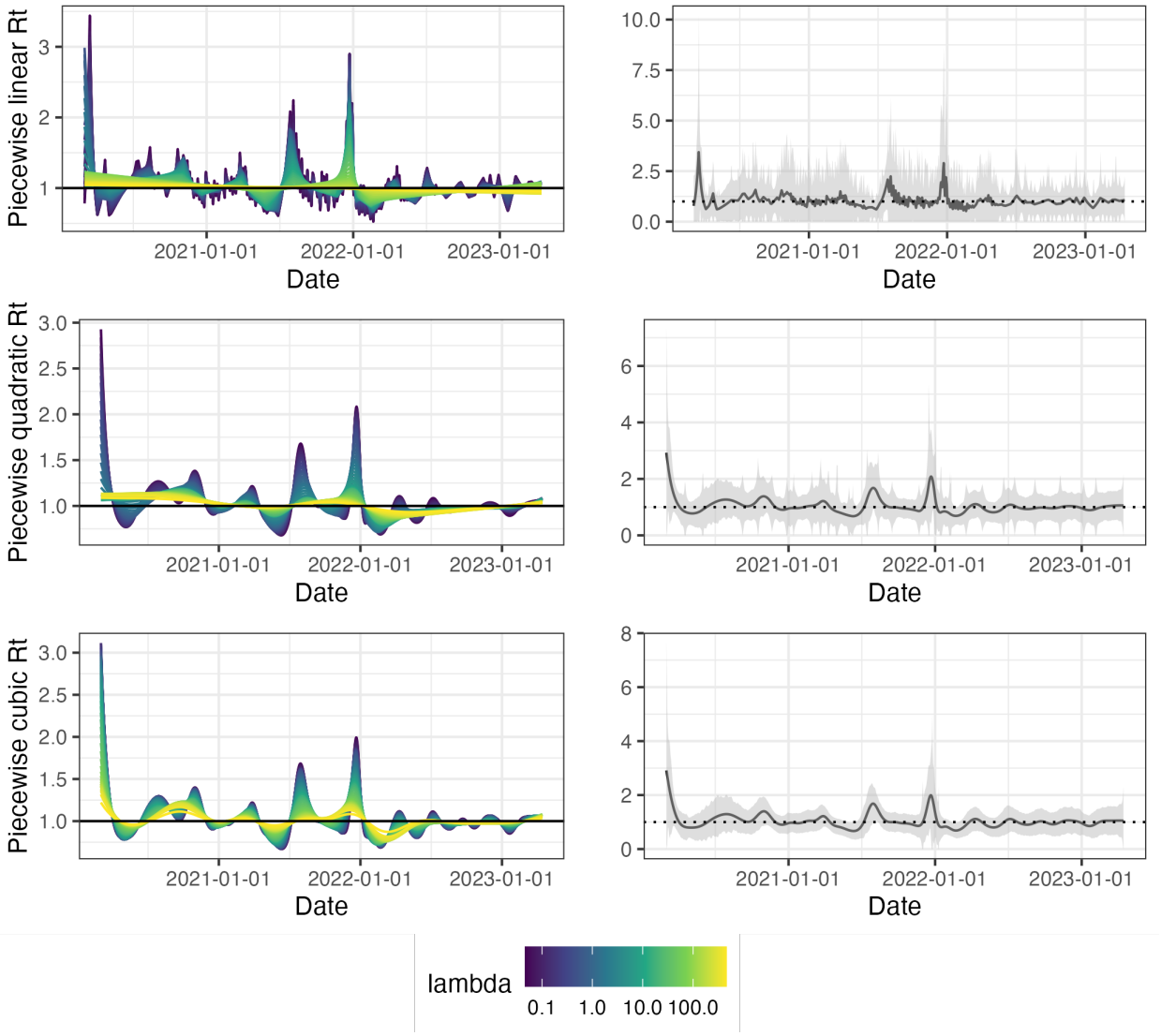

Figure 7: Estimated effective reproduction numbers for Covid19 daily confirmed counts between March 1st, 2020 and April 15th, 2023 in British Columbia, Canada. The left panels demonstrate estimates corresponding to 50 tuning parameters. The right panels display the CV-tuned estimates with 95% confidence intervals. The top, medium and bottom panels illustrate the estimated reproduction numbers ($\mathcal{R}_t$) using the Poisson trend filtering (in Equation (4)) with degrees $k = 1, 2, 3$ respectively.

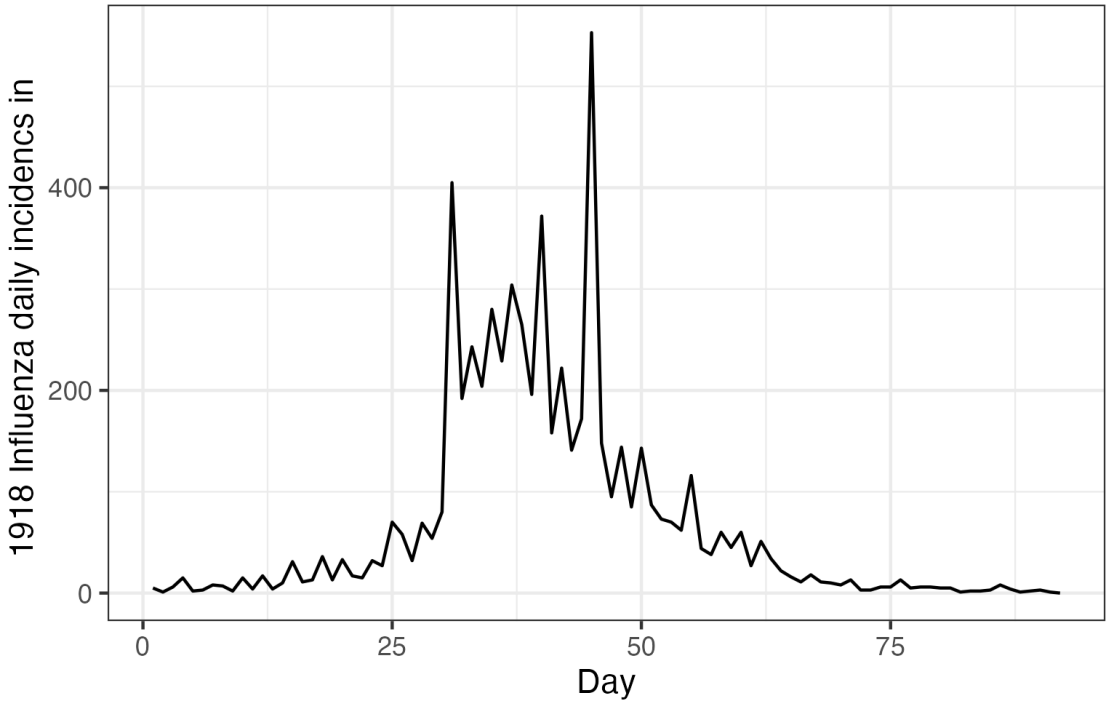

Figure 8: Daily influenza incidence counts in Baltimore, Maryland between September and November in 1918.

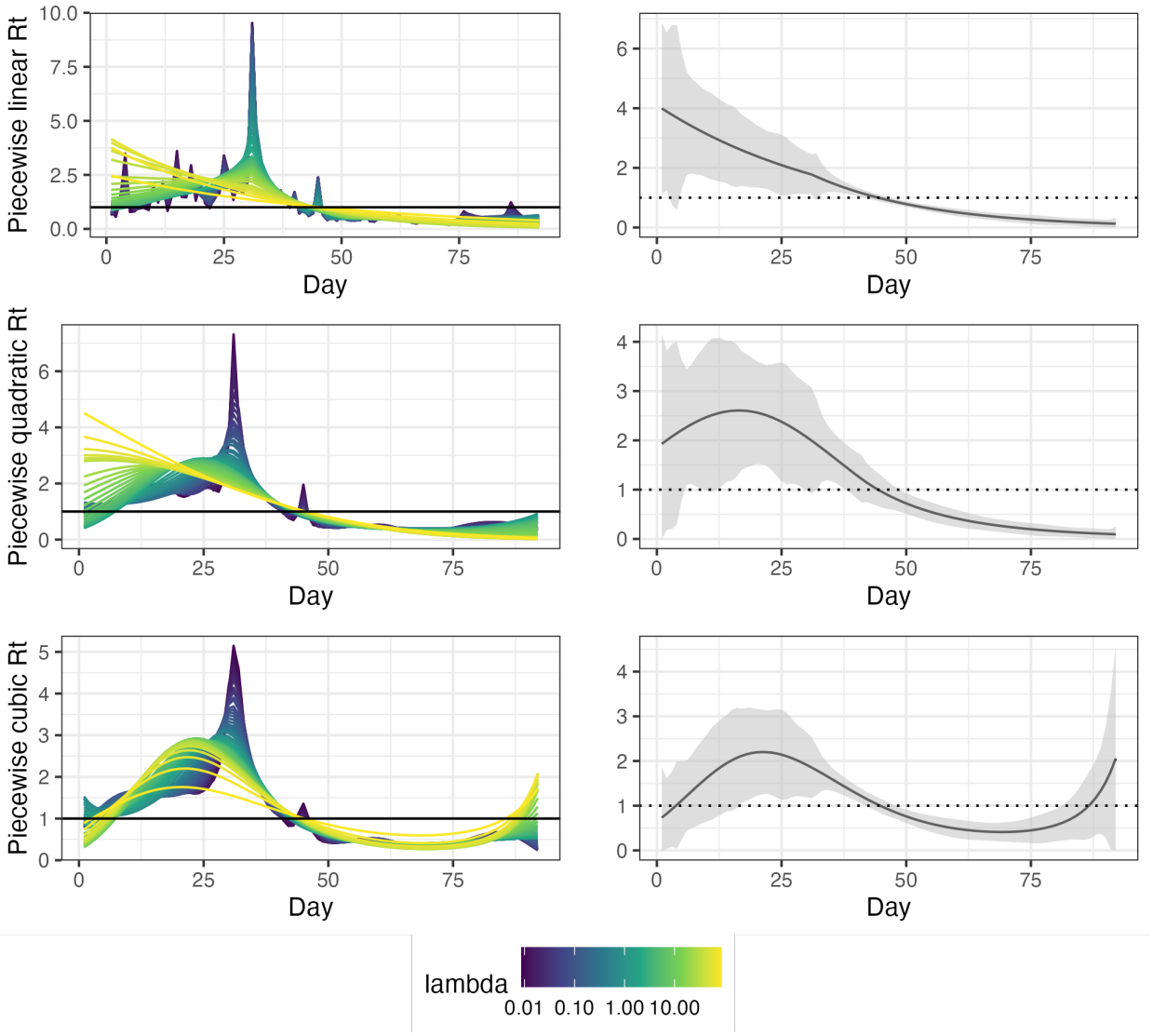

Figure 9: Estimated effective reproduction numbers for influenza in Baltimore, Maryland in 1918. The left panels show estimates for all 50 tuning parameters under consideration. The right column displays the CV-tuned estimates with 95% confidence bands. The rows (top to bottom) show estimated reproduction numbers ($\mathcal{R}_t$) using the Poisson trend filtering (in Equation (4)) with degrees $k = 1, 2, 3$ respectively.